Automated Segmentation of the Choroid from Clinical SD-OCT

Li Zhang,[1] *Kyungmoo Lee,*[1,2] *Meindert Niemeijer,*[2,6] *Robert F. Mullins,*[2,3] *Milan Sonka,*[1,2] *and Michael D. Abràmoff*[1–6]

Purpose. We developed and evaluated a fully automated 3-dimensional (3D) method for segmentation of the choroidal vessels, and quantification of choroidal vasculature thickness and choriocapillaris-equivalent thickness of the macula, and evaluated repeat variability in normal subjects using standard clinically available spectral domain optical coherence tomography (SD-OCT).

Methods. A total of 24 normal subjects was imaged twice, using clinically available, 3D SD-OCT. A novel, fully-automated 3D method was used to segment and visualize the choroidal vasculature in macular scans. Local choroidal vasculature and choriocapillaris-equivalent thicknesses were determined. Reproducibility on repeat imaging was analyzed using overlapping rates, Dice coefficient, and root mean square coefficient of variation (CV) of choroidal vasculature and choriocapillaris-equivalent thicknesses.

Results. For the 6×6 mm^2 macula-centered region as depicted by the SD-OCT, average choroidal vasculature thickness in normal subjects was 172.1 μm (95% confidence interval [CI] 163.7–180.5 μm) and average choriocapillaris-equivalent thickness was 23.1 μm (95% CI 20.0–26.2 μm). Overlapping rates were 0.79 ± 0.07 and 0.75 ± 0.06, Dice coefficient was 0.78 ± 0.08, CV of choroidal vasculature thickness was 8.0% (95% CI 6.3%–9.4%), and of choriocapillaris-equivalent thickness was 27.9% (95% CI 21.0%–33.3%).

Conclusions. Fully automated 3D segmentation and quantitative analysis of the choroidal vasculature and choriocapillaris-equivalent thickness demonstrated excellent reproducibility in repeat scans (CV 8.0%) and good reproducibility of choriocapillaris-equivalent thickness (CV 27.9%). Our method has the potential to improve the diagnosis and management of patients with eye diseases in which the choroid is affected. (*Invest Ophthalmol Vis Sci.* 2012;53:7510–7519) DOI:10.1167/iovs.12-10311

From the [1]Department of Electrical and Computer Engineering, University of Iowa, Iowa City, Iowa; the [2]Department of Ophthalmology and Visual Sciences, University of Iowa Hospitals and Clinics, Iowa City, Iowa; the [3]Institute for Vision Research, University of Iowa, Iowa City, Iowa; the [4]Department of Veterans Affairs, Iowa City Veterans Administration Medical Center, Iowa City, Iowa; the [5]Department of Biomedical Engineering, University of Iowa, Iowa City, Iowa; and [6]IDx LLC, Iowa City, Iowa.

Supported by Grants NEI-EY019112 and R01 EY018853 (MDA and MS), NEI-EY017451 (RFM), and NEI-EY017066 (MDA) and VA 1I01CX000119.

Submitted for publication June 1, 2012; revised August 22 and September 24, 2012; accepted October 3, 2012.

Disclosure: **L. Zhang**, None; **K. Lee**, None; **M. Niemeijer**, None; **R.F. Mullins**, None; **M. Sonka**, P; **M.D. Abràmoff**, P

Corresponding author: Michael D. Abràmoff, Department of Ophthalmology and Visual Sciences, University of Iowa Hospitals and Clinics, 200 Hawkins Drive, Iowa City, IA 52242; michael-abramoff@uiowa.edu.

The choroid is a vascular plexus between the retina and sclera that forms a vascular system with the highest flow of any tissue in the human body, and is crucial for oxygenation and metabolic activity of the RPE and outer retina.[1] Anatomically, the choroid can be divided into two principal components: the choriocapillaris, a lobular, vascular plexus comprised of large fenestrated capillaries adjacent to Bruch's membrane, and the choroidal stroma.[2] Most of the choroidal vasculature thickness is attributable to the choroidal stroma, which is comprised of larger vessels that supply and drain the choriocapillaris, as well as melanocytes, fibroblasts, immune cells, neurons, and ground substance that contribute to its thickness.[1]

The choroid is affected in many diseases of the retina.[3] Changes in the health of the choroid have been documented in early macular degeneration and in advanced disease.[4–6] Decreased choroidal vasculature thickness has been described in age-related macular degeneration,[7] although it has not been observed universally. Some choroidal thinning occurs during normal aging, and is seen acutely in some patients in a condition referred to as age-related choroidal atrophy.[8] Other conditions, such as central serous retinopathy,[9] polypoidal choroidal vasculopathy, and inflammatory conditions, such as in choroiditis and autoimmune diseases, are associated with thickening of the choroid.

Historically, imaging the choroid in patients was possible with indocyanine green (ICG) angiography, where injection of this fluorescent dye and subsequent imaging of fluorescence allowed two-dimensional (2D) imaging of the choroid pattern, and the existence of leakage and vessel wall abnormalities.[10] ICG may be useful clinically in a range of choroidal diseases, though recent studies have failed to demonstrate this.[11] However it does not depict the 3-dimensional (3D) structure of the choroid. Several studies, therefore, have used spectral domain optical coherence tomography (SD-OCT), which allows 3D imaging of the posterior eye, including the choroid,[12] and used manual or semi-manual methods to quantify choroidal vasculature thickness.[13,14] However, such methods suffer from large intra- and inter-observer variability, and do not have access to the choriocapillaris separately. We previously developed and validated fully automated, highly robust, and 3D segmentation of retinal structures.[15]

The purpose of our study was to develop and evaluate a fully automated 3D method for segmentation of the choroidal vessels, and quantification of choroidal vasculature thickness and choriocapillaris-equivalent thicknesses of the macula in normal subjects, using standard clinically available SD-OCT.

Methods

Subject and Data Collection

Normal subjects were recruited by advertising, and were included in this prospective study after written informed consent. All subjects

Investigative Ophthalmology & Visual Science, November 2012, Vol. 53, No. 12

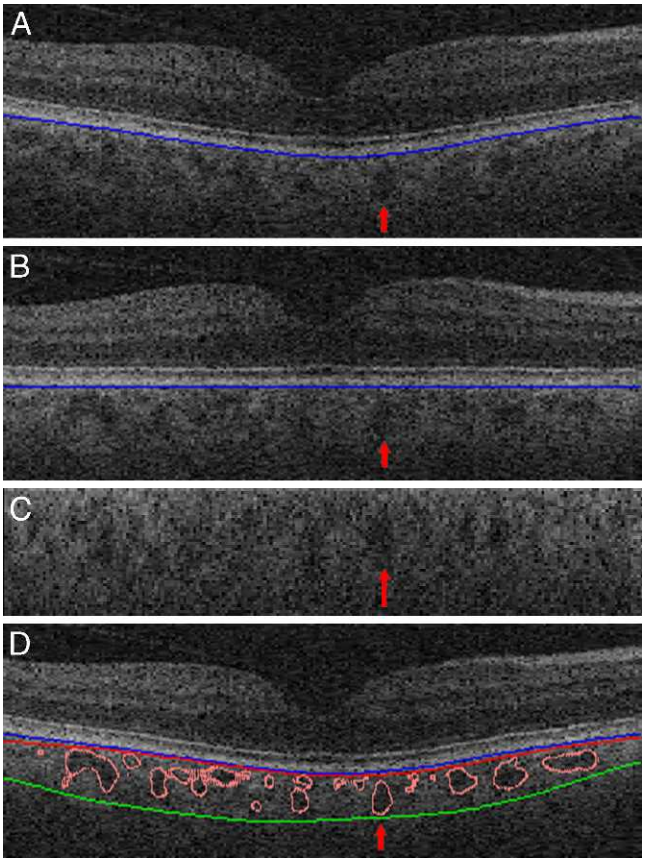

Figure 1. Choroidal vasculature in standard clinical OCT scan, central B-scan shown. (**A**) Original OCT volume with segmented Bruch's membrane (*blue line*). (**B**) Flattened OCT volume with segmented Bruch's membrane. (**C**) Subvolume under Bruch's membrane containing the entire choroid. (**D**) Original OCT volume with superimposed segmented vessels (*pink outlines*), segmented Bruch's membrane (*blue line*), and the top (*red line*) and bottom surfaces (*green line*) fitting around the choroidal vasculature, used to determine choroidal vasculature thickness and choriocapillaris-equivalent thickness. *Red arrow* points to one of the choroidal vessels.

were imaged twice on the same day, and macula-centered SD-OCT volumes (Zeiss Cirrus; Carl Zeiss Meditec, Inc., Dublin, CA) were obtained from each subject in both eyes; a single eye was selected randomly for further analysis. Each volume was 200 (width of B-scan) $\times$ 200 (number of B-scans) $\times$ 1024 (depth, or height of B-scan) voxels, corresponding to physical dimensions of $6 \times 6 \times 2$ mm^3, and voxel size was $30 \times 30 \times 2$ μm^3. Volume scan data were de-identified before further image analysis. Institutional Review Board of the University of Iowa gave approval to the study, which adhered to the tenets of the Declaration of Helsinki.

OCT Volume Flattening and Choroidal Layer Extracting

Due to the relative position of the OCT scanner and patient's pupil, and variation in eye movements, the raw OCT image data are deformed randomly. To reduce the geometric distortion of the choroidal layer, a volume flattening process was needed. Thus, the OCT volume first was segmented automatically using our reported graph-based multilayer segmentation approach,[16] which produced the segmentation result of 11 intraretinal surfaces, including Bruch's membrane (BM, Fig. 1A). The entire raw OCT volume then was flattened based on the segmented BM surface (Fig. 1B). The choroidal layer was assigned the position beneath Bruch's membrane. A sufficiently large subvolume containing choroidal layer (Fig. 1C) was selected as the target region to use our choroidal vasculature segmentation method.

Preprocessing of SD-OCT Volumes

Due to the OCT imaging physics, silhouettes occur in the regions under the retinal vessels (Fig. 2A). We introduced a three-stage approach to change the contrast of the silhouette regions in the choroidal layer and to reduce the likelihood of incorrect segmentation due to retinal vessel silhouettes. In the first stage, two of the 11 segmented surfaces, as labeled in Figure 2B, were used to define the RPE complex. From top to bottom, the yellow-marked surface is between the inner segment layer and connecting cilia, and the green-marked surface is Bruch's membrane. In the second stage, a projection image was created by computing the mean intensity values of voxels within the RPE (Fig. 2C). Retinal vessel silhouettes were then segmented using our previously published retinal vessel segmentation approach (Fig. 2D).[17] The retinal vessel silhouettes are visible in the RPE and choroidal layers. As such, the retinal vessel silhouettes must be identified and distinguished from the similar-looking signatures of choroidal vessels. Therefore, in the third stage, the identified retinal vessel silhouettes were used as a mask, based on which the contrast of the OCT data was smoothed so that the retinal vessels would not show among the identified choroidal vessels.

Choroidal Vasculature Segmentation

The choroidal vasculature segmentation consists of two main steps: vessel detection and vessel segmentation. In the vessel detection step, choroidal vessels were modeled as 3D tube-like objects in a resampled subvolume that yielded isometric (cubic) voxels. To detect choroidal vessel voxels, we applied a multiscale Hessian matrix analysis[18–20] on the selected subvolume: a 3×3 tensor matrix was generated for each voxel, containing local directionality and shape information. The vesselness map of the choroidal vasculature then was calculated using the eigenvectors of the tensor matrix at each voxel position. For the second main step of vessel segmentation, voxel groups with relatively high vesselness values were selected by thresholding of the vesselness map using an experimentally-determined threshold that was fixed for all analyzed images. Varying this threshold gave close-to-equivalent results over a large range of values. The resulting binary regions were used as seeds for a classic region growing approach to segment the choroidal vasculature (Figs. 1D, 3).

Choroidal and Choriocapillaris-Equivalent Thickness Maps

After choroidal vasculature segmentation, a thin plate spline (TPS) approach[21] was applied to the flattened segmentation result to envelop the upper and lower surfaces of the choroidal vasculature segmentation result (Fig. 4). The choroidal vasculature thickness is defined as the Euclidean distance between these two surfaces. To measure the choriocapillaris-equivalent thickness, Bruch's membrane surface was used as a reference surface for the boundary of the entire choroid, including the choriocapillaris. The choriocapillaris-equivalent thickness then was defined as the distance between Bruch's membrane and the upper surface of the choroid-equivalent region as defined above. Finally, the choroidal vasculature thickness was defined as the distance between Bruch's membrane and the lower surface of the choroidal vasculature. Choroidal vasculature and choriocapillaris-equivalent thickness maps were created for all subjects. The relationship of age to choroidal vasculature thickness and choriocapillaris-equivalent thickness was analyzed using scatter plots. Coefficients of variation (CV) were calculated using the root mean square (RMS) approach, and mean and 95% confidence intervals (CI) are reported. We calculated the volume (in mm^3) of the choroidal vasculature in the 6×6 mm^2 macula-centered region to evaluate the segmentation quality.

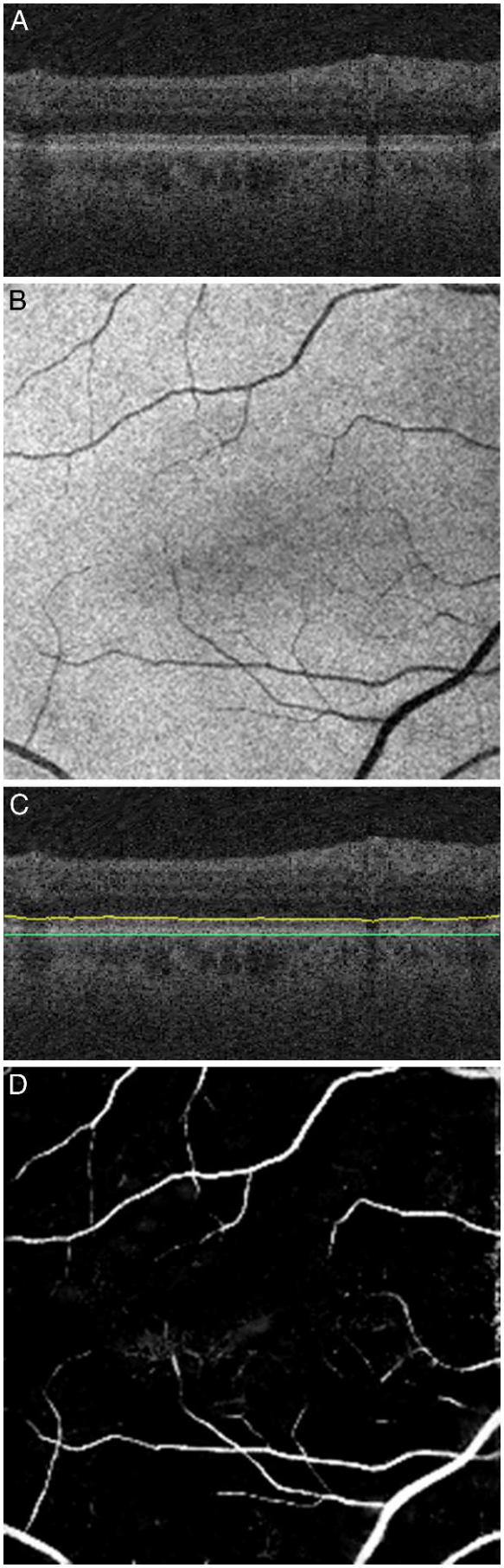

Reproducibility Analysis of the Choroidal Vasculature Segmentation

Reproducibility analysis of the choroidal vasculature segmentation was performed on repeat scans of the same eye. To align the corresponding volumes from the same subject for further analysis, the two volumetric scans were registered automatically using 2D retinal vessel segmentation and affine registration (Niemeijer M, et al. *IOVS* 2011;52:ARVO E-Abstract 1304; Fig. 5). After the volumes were registered for each subject, three reproducibility indices of the choroidal vessel segmentation were introduced: overlapping rate, skeletonized overlapping rate, and Dice coefficient. These three indices yield unity for the best reproducibility and null for the worst reproducibility; their definitions follow.

Overlapping Rate. Overlapping rate, $Overlap_{total}$, was computed from the two choroidal vasculature segmentation results as:

$$Overlap_{1st} = \frac{|Vol_{1st}| \bigcap |Vol_{2nd}|}{|Vol_{1st}|},$$

$$Overlap_{2nd} = \frac{|Vol_{1st}| \bigcap |Vol_{2nd}|}{|Vol_{2nd}|},$$

$$Overlap_{total} = \frac{Overlap_{1st} + Overlap_{2nd}}{2},$$

where $|Vol_{1st}|$ represents the choroidal vasculature segmentation result of the first imaging session data, and $|Vol_{2nd}|$ represents the choroidal vasculature segmentation result of the second session data.

Skeletonized Overlapping Rate. To evaluate further the accuracy of the proposed method, central lines of the choroidal vasculature segmentation (skeletons) were generated by using the Insight Segmentation and Registration Toolkit (available online at http://www.itk.org/). Even though the two volumes were registered, slight shift errors still may occur. Although nonaffine registration can correct such errors, the required warping of one volume would result in overestimating the correctness of the registration. Therefore, we used only affine registration (translation and rotation) and introduced a narrow-neighborhood band of insensitivity to disregard these small distances between the skeletonization results caused by imperfect registration.

Dice Coefficient. The Dice coefficient[22] of the overlap between the two choroidal vasculature segmentation results also was calculated, as yet another metric. The Dice coefficient is defined as follows:

$$DiceCoef = \frac{2(|Vol_{1st}| \bigcap |Vol_{2nd}|)}{|Vol_{1st}| + |Vol_{2nd}|},$$

where $|Vol_{1st}|$ and $|Vol_{2nd}|$ were defined above (Fig. 9).

Results

In our study, 43 normal subjects were repeat scanned, and in 24/43 subjects choroidal vessel fraction and the volume of choroidal vasculature in both repeat scans were sufficient for further analysis, even where visual inspection shows little detail of the choroidal vessels in B-scans (Fig. 1D). In these 24 subjects, average volume of choroidal vasculature was 1.12 mm^3 (95% CI 1.04–1.19 mm^3), and they were included in the

Figure 2. Detection of retinal vessel silhouettes. (**A**) Example x-z slice with retinal vessel silhouettes (*colored arrows*). (**B**) Projection image defined by the mean intensity value inside the RPE along the z direction showing vessel silhouettes (same as in [**A**]). (**C**) Reference surfaces (*yellow and green lines*). (**D**) 2D retinal vesselness map.

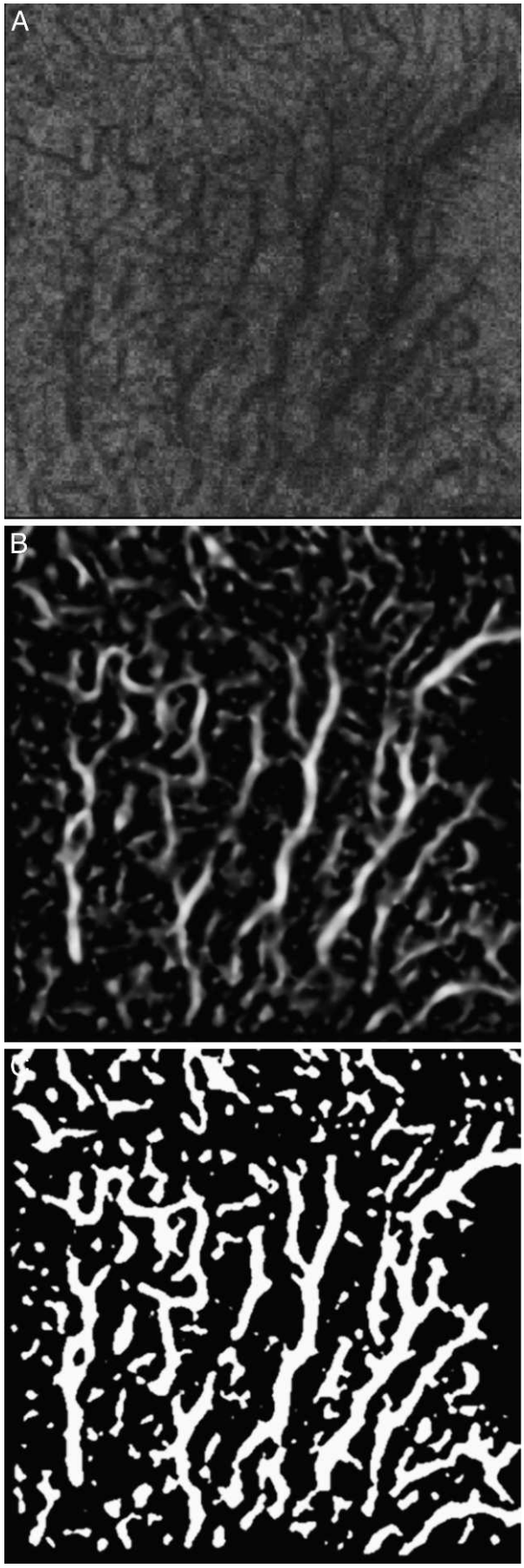

study. In 19/43 subjects, one or both repeat scans had insufficient volume of the choroidal vasculature and these subjects were excluded from the study; average volume of choroidal vasculature was 0.58 mm^3 (95% CI 0.48–0.67 mm^3). Mean age for the 24 subjects where both scans could be analyzed was 43.96 (± 19.18 SD, minimum 11 years, maximum 75 years), and 5 were male and 19 female subjects. Choroidal vasculature segmentation was applied to all volume sets. Figures 7A to 7C show the x-y slice (projection direction) examples of the flattened subvolume and vessel segmentation result. Figure 7D shows a 3D visualization example of the choroidal vasculature segmentation. The minimal diameter of choroidal vessels thus segmented was approximately 60 μm, and the maximal diameter was approximately 180 μm. The volume of choroidal vasculature in OCT scans that currently can be analyzed successfully by our method is different from those that contain OCT image data unsuitable for analysis, and Figure 6 shows an example of one of the scans from the 19/43 subjects where the volume of the detected vasculature is markedly and quantifiably lower than that of analyzable OCT images, such as in Figure 7D.

For the 6×6 mm^2 macula-centered region as imaged by the SD-OCT, average choroidal vasculature thickness was 172.1 μm (95% CI 163.7–180.5 μm) and average choriocapillaris-equivalent thickness was 23.1 μm (95% CI 20.0–26.2 μm). These values are comparable to histologic findings of human choriocapillaris.[4,5] The scatter plots of average choroidal vasculature thickness and average choriocapillaris-equivalent thickness are shown in Figure 8. In this small set of normal subjects, choroidal vasculature thickness decreased with age at a rate of 0.72 μm per year and choriocapillaris-equivalent thickness decreased at 0.25 μm per year.

Reproducibility tests were applied to all 24 subjects (Fig. 9). In all cases, a 2-pixel narrow band of distance insensitivity was used. The average overlapping rate was 0.79 ± 0.07. The mean skeletonized overlapping rate was 0.75 ± 0.06. Average Dice coefficient was 0.78 ± 0.08. Choroidal vasculature thickness RMS CV was 8.0% (95% CI 6.3%–9.4%), while choriocapillaris-equivalent thickness CV was 27.9% (95% CI 21.0%–33.3%).

Discussion

The results of our pilot study showed a fully automated 3D method capable of segmenting the choroidal vessels, as well as of quantifying choroidal vasculature thickness and choriocapillaris-equivalent thickness. Volume of the choroidal vasculature allowed automatic separation of those subjects in which the OCT image quality was too low to detect any choroidal vessels. The method works on standard clinically available SD-OCTs devices, in this study the Zeiss Cirrus. The reproducibility of the automated method was high, as shown by overlapping and skeletonized overlapping rates of 0.79 and 0.75, Dice coefficient of 0.78, and CVs of 8.0% for choroidal vasculature thickness. Choriocapillaris-equivalent thickness measures were more variable with an average CV of 27.9%. We confirmed that choroidal vasculature thickness and choriocapillaris-equivalent thickness decrease with age, as was found in earlier studies (for total thickness) using different manual techniques.[6,13]

Figure 3. Choroidal vasculature segmentation compared to projection of the flattened choroidal layer. (**A**) An x-y projection view of flattened data. (**B**) Corresponding x-y projection at the same z-level of the vesselness map. (**C**) Corresponding x-y projection at the same z-level of the choroidal vasculature segmentation.

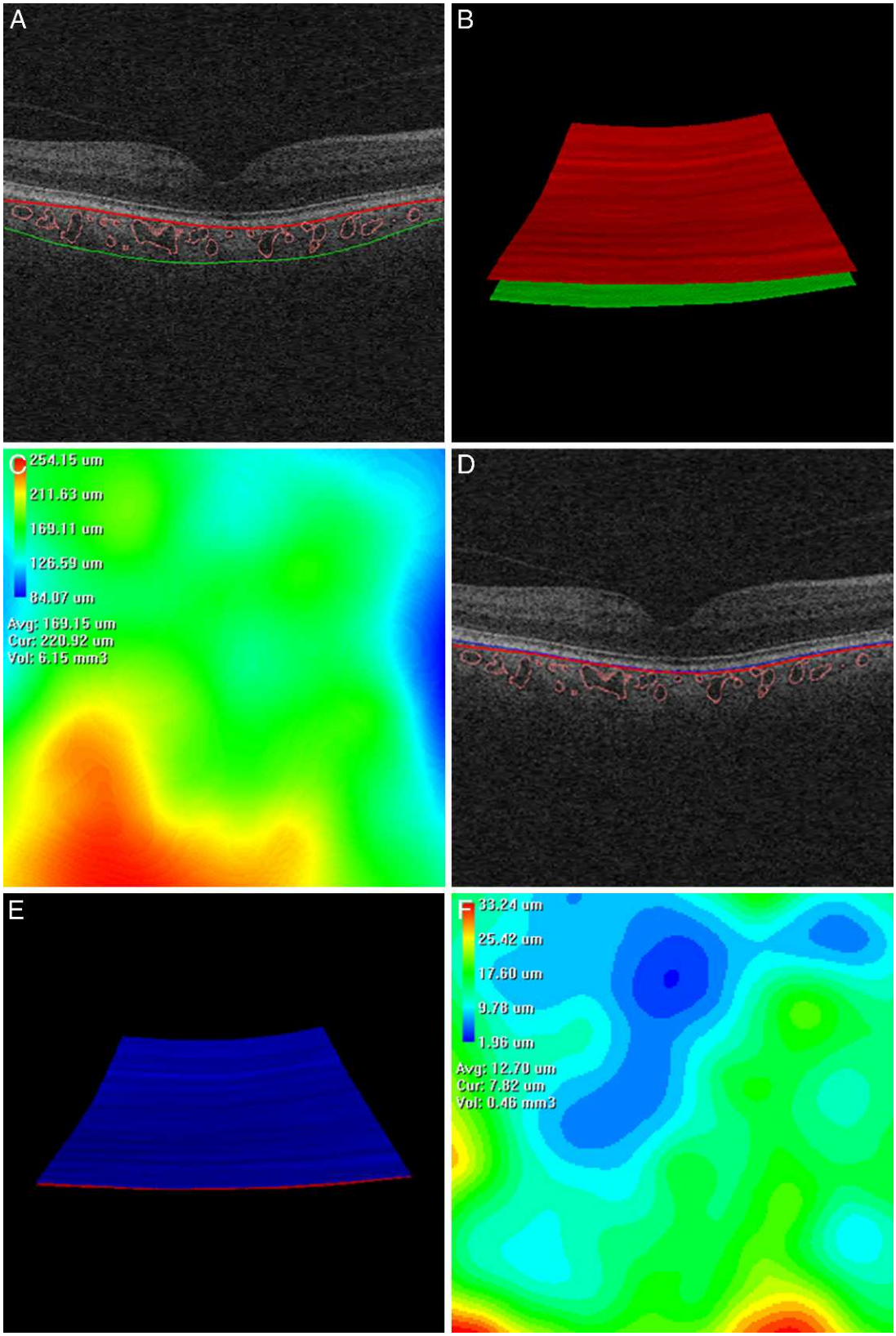

Figure 4. Upper and lower surfaces of the choroidal vasculature, used to determine choroidal vasculature thickness and choriocapillaris-equivalent thickness. (**A**) Upper surface and lower surface of the segmented choroidal vasculature in one B-scan. (**B**) 3D visualization of the two surfaces as shown in (**A**). (**C**) Map of choroidal vasculature thickness. (**D**) Bruch's membrane and the upper surface of the segmented choroidal vasculature, indicating the boundaries of the choriocapillaris-equivalent region. (**E**) 3D visualization of the two surfaces shown in (**D**). (**F**) Choriocapillaris-equivalent thickness map.

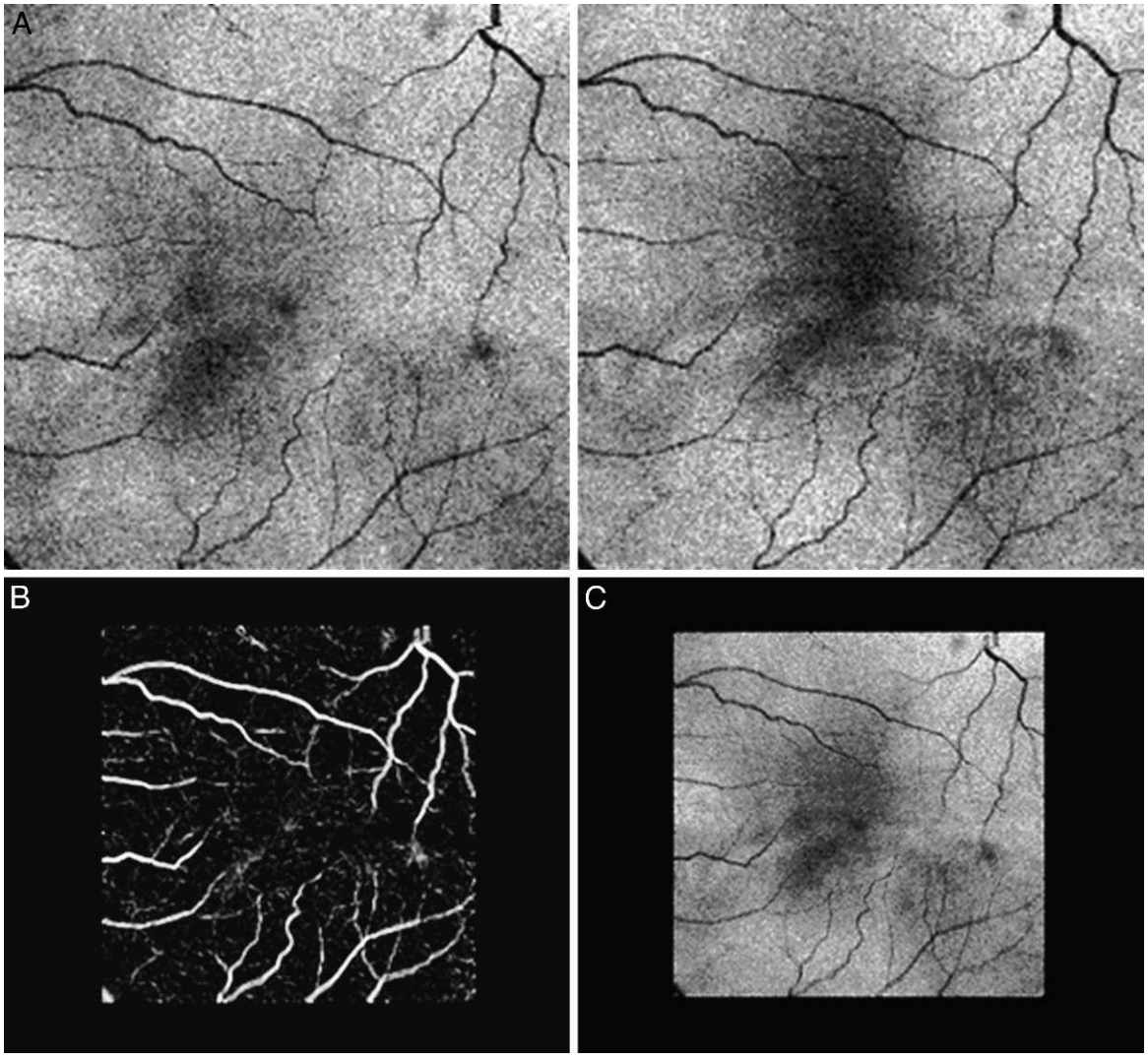

Figure 5. Automated retinal vessel based registration. (**A**) Two OCT projection images from two sequentially-obtained datasets of the same subject. (**B**) Registration of the retinal vessel segmentation, showing almost perfect match. (**C**) Registration of the two OCT projection images from two imaging sessions.

To the best of our knowledge, this is the first method to achieve segmentation of the choroid, including OCT equivalents of the outer choroidal vasculature as well as the choriocapillaris. In standard clinical SD-OCT, with axial resolution of 4 to 8 μm and x-y resolution of no better than 30 μm, individual capillaries in the choriocapillaris, while large compared to most capillary beds, cannot be resolved. However using our approach, we can estimate the thickness of a layer that does not contain larger choroidal vessels and is below Bruch's membrane. Though we expect this layer to be similar to the choriocapillaris, we took pains to call it the choriocapillaris-equivalent.

While the clinical use of segmenting the choroid, and measuring the choriocapillaris and choroidal vasculature locally is not clear at this time, as has been shown for ICG angiography,[11] we hypothesize that our method may clarify some of the inconsistencies in the literature about changes in the choroid in different disease states, since a more precise delineation of the different layers and the regional/local availability of measurements may reveal relationships that are difficult to observe when the entire choroid is summed.

Because we achieve true segmentation of the larger choroidal vessels, our method facilitates their 3D visualization. The resulting patterns are highly similar to those obtained in ICG angiography,[23] and those in postmortem alkaline phosphatase stained preparations and choroidal casts[4,24] (Fig. 10 for visual comparison of these vessel patterns).

A major concern in our study has been to validate the method. Though ICG angiography provides 2D projections of the choroidal vessel pattern, there are ethical concerns with administering ICG to normal subjects, because of the risk for an allergic response, anaphylactic shock, and even death.[25] Fundus photography occasionally may show the choroidal vessel pattern in specific regions, especially in lightly pigmented individuals. In our subjects, the choroidal pattern was visualized rarely well enough to be able to serve for validation. In addition, the OCT scans used in our study cover the area of 6×6 mm^2 centered on the fovea, which usually contains more pigment than the rest of the macula, so that prevents using fluorescein angiography for validation. Though the choroid can be cast in postmortem eyes, the retinal edema that occurs immediately after death prevents obtaining high

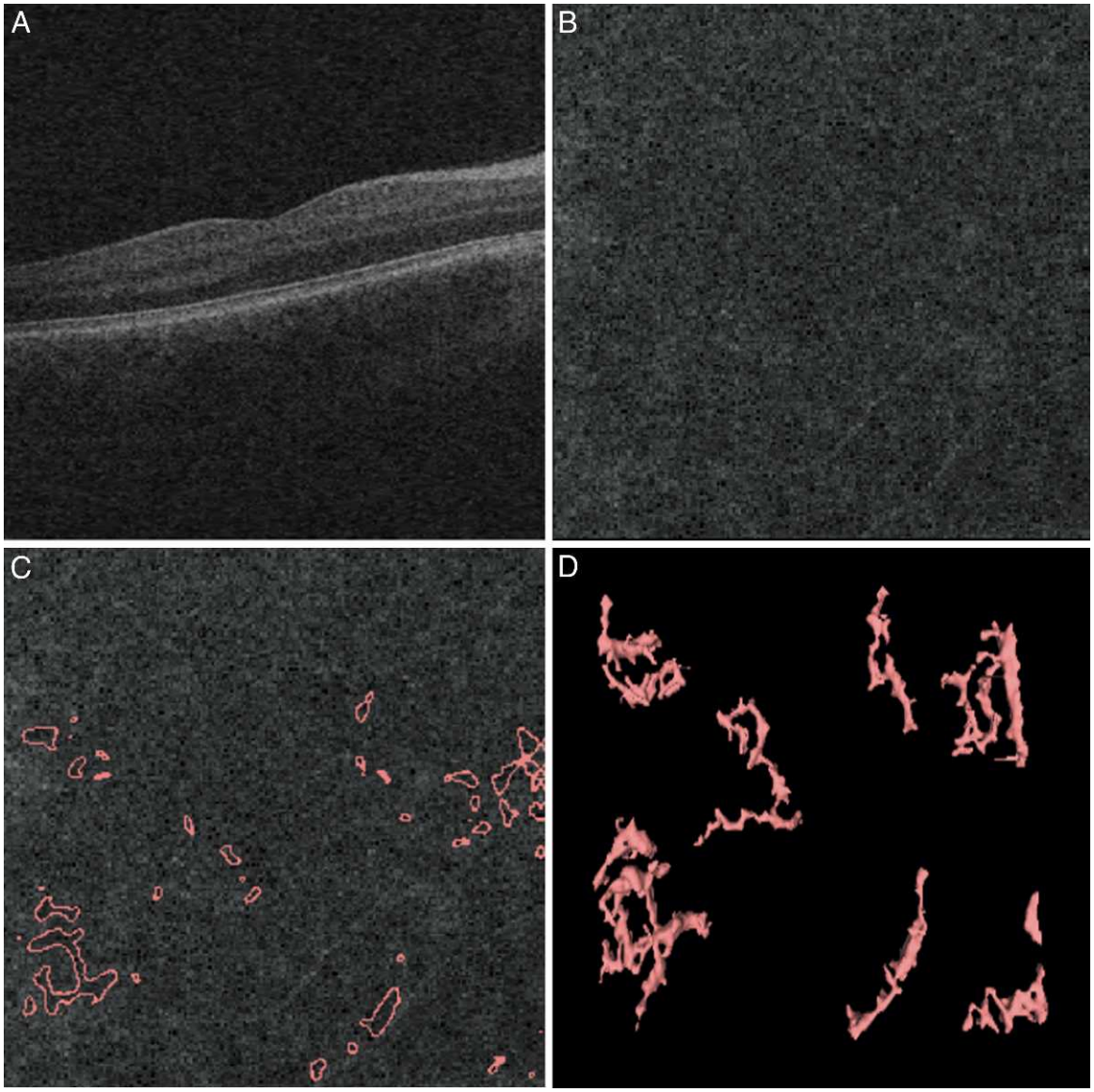

Figure 6. Example of OCT data with low volume of choroidal vasculature, unsuitable for segmentation and analysis of choroidal vasculature. (**A**) Central B-scan. (**B**) Example x-y slice of flattened OCT volume. (**C**, **D**) Silhouettes and surface rendering of the 3D segmentation of choroidal vasculature. Note the low volume of detected vessels compared to Figure 6D. This low volume of choroidal vasculature are used for automated labeling of nonanalyzable scans. The volume of the choroidal vasculature is 0.19 mm^3.

quality OCT scans, especially of the deeper layers. Thus, instead of comparing the results to an accepted reference standard, in our study we focused on analyzing the reproducibility of the method, using repeat scans taken on the same day and comparing the segmentations for repeat scans. We concluded that the reproducibility of choroidal vasculature thickness is excellent, while that of the choriocapillaris-equivalent is good. Clearly, our automated method is measuring a real structure, and comparison to well-known choroidal patterns strengthens the idea that the choroidal vasculature is indeed segmented.

Interestingly, our method shows that in the majority of normal subjects, most of the choroidal vasculature in the macula can be segmented successfully in standard clinical SD-OCT, even though cursory examination of B-scans shows very little contrast in this region (Fig. 1). Because of the large number of B-scans achievable with modern clinical SD-OCT, there is sufficient information for segmentation of the choroidal vessels as long as the 3D context is used. Achieving good performance likely depends on the x-y isotropy of the acquired images, meaning that the A-scans are spaced evenly in all directions, instead of having large numbers of A-scans in one direction and large spaces between the slices in another.[26]

Other studies also have estimated the thickness of the total choroid, between Bruch's membrane and the outermost part of the choroidal vessels. For example, Shin et al. found that the average thickness of the choroid was 285.9 $\pm$ 53.0 μm, thicker than the 193.1 μm (172.1 $\pm$ 21.0) that we report here.[13] The reason for this discrepancy is likely that Shin et al. measured the choroid as extending from Bruch's' membrane to the sclera, while we only measured the choroid extending as far as the vessel walls closest to the sclera. Thus, tissue of the suprachoroidea, present between the outer vessel walls and the sclera, is not included in our measure of choroidal vasculature thickness. We found that choroidal vasculature thickness decreases at a rate of 0.72 μm per year, which is

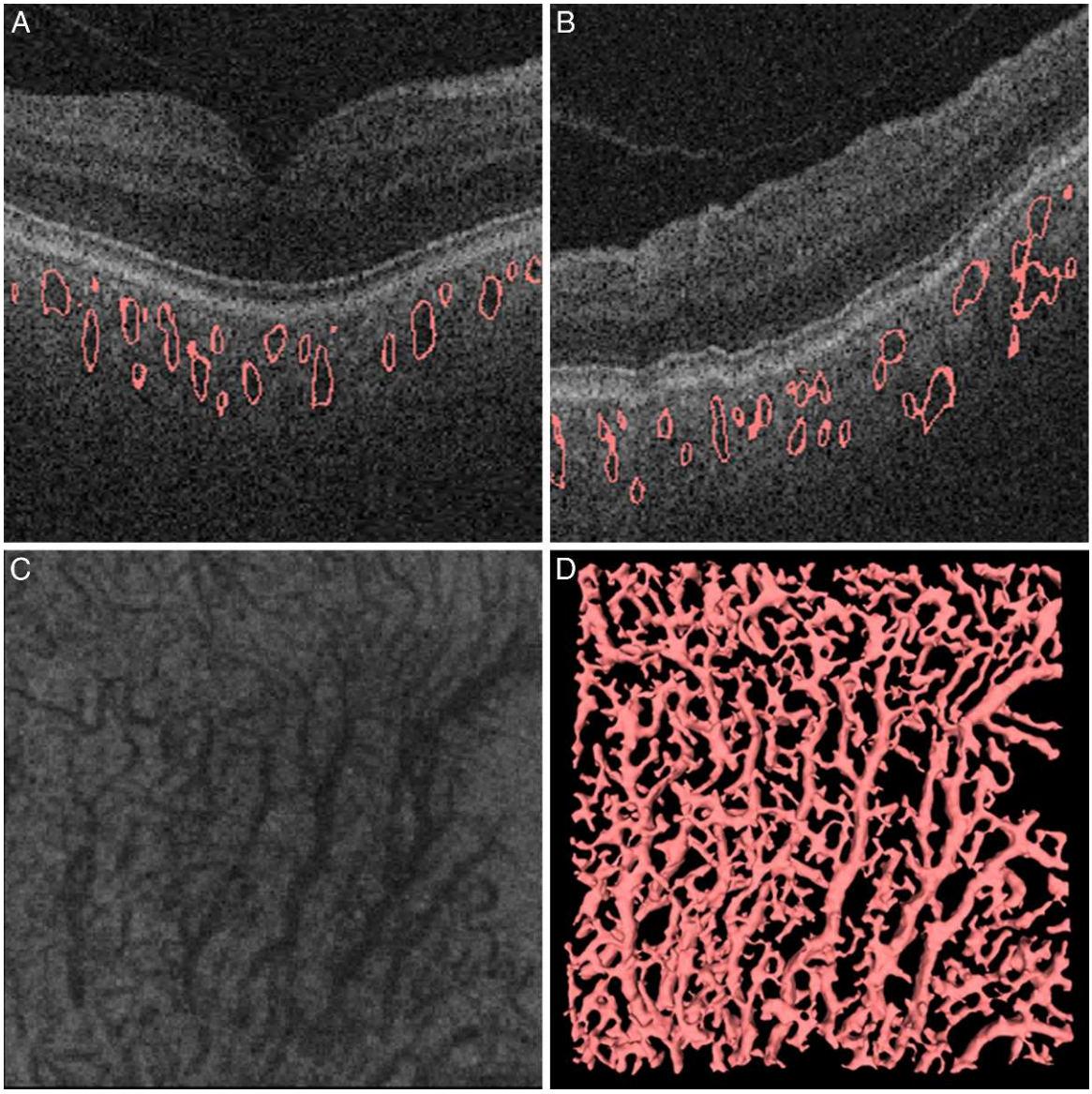

Figure 7. Visualization of choroidal vessel segmentation. Panels (**A**) and (**B**) show example x-z and y-z slices of the vessel segmentation result. (**C**) Example x-y slice of flattened OCT volume. (**D**) Surface rendering of 3D segmented choroidal vasculature. The volume of the choroidal vasculature is 1.15 mm^3.

comparable to 0.97 μm per year found by Shin et al., and 1.4 to 1.56 μm per year using different approaches of Agawa et al. and Ikuno et al.[27,28] In a study of 34 normal subjects and 19 patients with cataracts, these investigators compared choroidal thickness maps, using manual expert segmentation, from standard clinical (Cirrus) OCT and experimental swept source 1060 nm OCT, and showed that swept source OCT results in higher-quality maps, especially in eyes with cataracts.[29] Our approach for automated segmentation with low inter-visit variability can be expected to perform better, that is, yield fewer failed segmentations, in swept source OCT as well. In a study of 3 normal subjects, swept source 1060 nm OCT was used, and manually segmented maps of choriocapillaris (CC), Sattler's layer (SL), Haller's layer (HL), and lamina suprachoroidea layer (LSL) were obtained successfully.[12] Using 840 nm SD-OCT images limits the imaged depth of the choroid and, thus, limits choroidal segmentation to what can be visualized. Our choriocapillaris equivalent is equivalent to the choriocapillaris layer, our choroidal vasculature is equivalent to Sattler's and Haller's layers; both have corresponding thicknesses as noted by Motoghianzam et al.[12] The lamina suprachoroidea layer cannot be visualized using 840 nm SD-OCT and so it was not segmented in our study.

There are some limitations to this pilot study of a fully automated 3D method for segmentation of the choroidal vessels. First of all, the number of subjects was relatively small. We currently are pursuing a study in a much larger population, as well as in patients with various retinal abnormalities.

Second, we achieved successful segmentation for two repeat scans in just over half, 24/43 subjects, while 19 of 43 subjects needed to be excluded because at least one OCT volume had insufficient image quality for further analysis. Choroidal vessel fraction and the volume of choroidal vasculature allow sufficient OCT quality to be determined automatically. Possibly, enhanced depth imaging and a longer center wavelength (with these scans, 840 nm), such as 1060

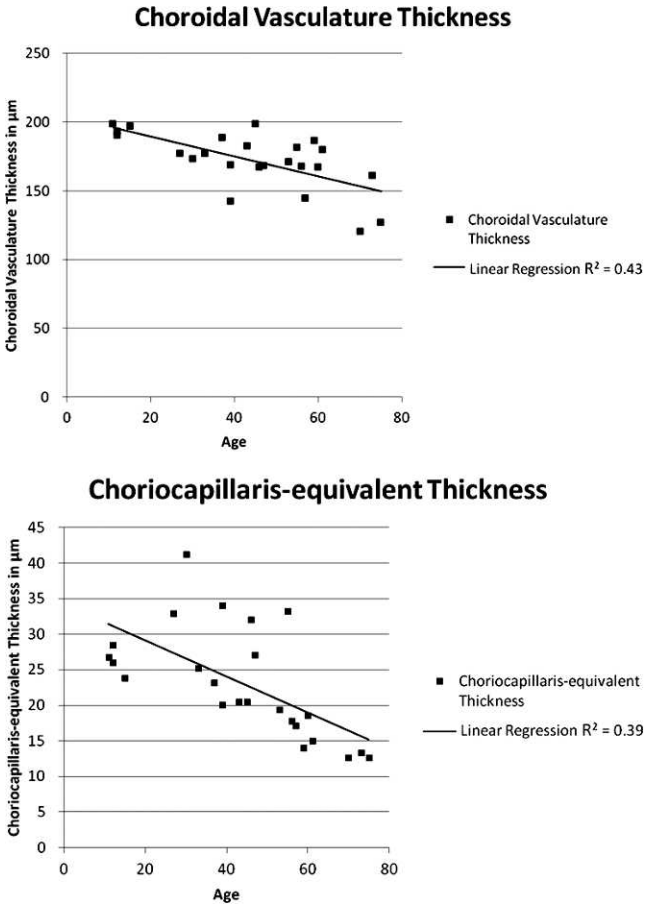

Figure 8. Relationship of choroidal vasculature thickness (*top*) and choriocapillaris-equivalent thickness (*bottom*) to age in normal subjects.

nm, that penetrates deeper, may allow a larger percentage of subjects to be measured successfully.[30]

Third, we have studied only reproducibility in normal subjects. In subjects with less normal choroid, such as those suffering from macular degeneration or choroiditis, the measurement reproducibility may well be less favorable.

In summary, we developed and validated a fully automated 3D method capable of segmentation of the choroidal vessels, as well as quantification of choroidal vasculature thickness and choriocapillaris-equivalent thickness. The method works on standard clinically available SD-OCT devices, in this study the Zeiss Cirrus, and has good reproducibility, as shown from the repeat-variability studies. Potentially, our method may improve the diagnosis and management of patients with eye diseases in which the choroid is affected.

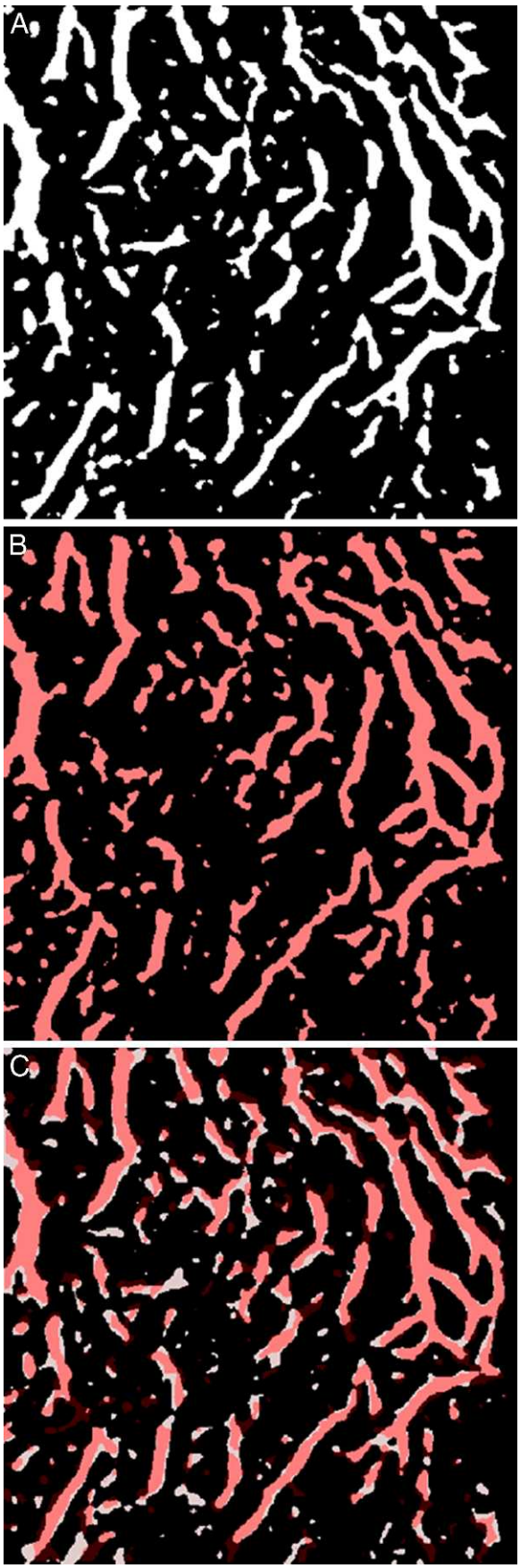

Figure 9. Dice analysis of reproducibility of choroidal vasculature segmentation. (**A**) x-y slice of choroidal vasculature segmentation from the first scan of a subject, choroidal vessels in *white*. (**B**) x-y slice at the same z-level of the choroidal vasculature segmentation in the repeat, second, scan of the same subject, after affine registration to the first, with choroidal vessels in *red*. (**C**) Overlay of the two choroidal vessel segmentations, where *pink areas* indicate overlapping choroidal vessels in both scans, *black* depict areas with no choroidal vessels, and *white* and *red areas* where choroidal vasculature was segmented in first and second scans, respectively.

Figure 10. Human choroidal vasculature imaged by endogenous alkaline phosphatase activity, using the method described by McLeod and Lutty.[4] Note the large vessels in the choroidal stroma, segmented by our method and the more superficial, smaller choriocapillaris vessels are visible as overlaid.

References

1. Nickla DL, Wallman J. The multifunctional choroid. *Prog Retin Eye Res*. 2010;29:144–168.
2. Hogan MJ, Alvarado JA, Weddell JE. *Histology of the Human Eye*. Philadelphia, PA: W.B. Saunders Co.; 1971.
3. Zarbin MA. Current concepts in the pathogenesis of age-related macular degeneration. *Arch Ophthalmol*. 2004;122: 598–614.
4. McLeod DS, Grebe R, Bhutto I, Merges C, Baba T, Lutty GA. Relationship between RPE and choriocapillaris in age-related macular degeneration. *Invest Ophthalmol Vis Sci*. 2009;50: 4982–4991.
5. Mullins RF, Johnson MN, Faidley EA, Skeie JM, Huang J. Choriocapillaris vascular dropout related to density of drusen in human eyes with early age-related macular degeneration. *Invest Ophthalmol Vis Sci*. 2011;52:1606–1612.
6. Ramrattan RS, van der Schaft TL, Mooy CM, de Bruijn WC, Mulder PG, de Jong PT. Morphometric analysis of Bruch's membrane, the choriocapillaris, and the choroid in aging. *Invest Ophthalmol Vis Sci*. 1994;35:2857–2864.
7. Jirarattanasopa P, Ooto S, Nakata I, et al. Choroidal thickness, vascular hyperpermeability, and complement factor H in age-related macular degeneration and polypoidal choroidal vasculopathy. *Invest Ophthalmol Vis Sci*. 2012;53:3663–3672.
8. Spaide RF. Age-related choroidal atrophy. *Am J Ophthalmol*. 2009;147:801–810.
9. Wang M, Munch IC, Hasler PW, Prünte C, Larsen M. Central serous chorioretinopathy. *Acta Ophthalmol*. 2008;86:126–145.
10. Yannuzzi LA. Indocyanine green angiography: a perspective on use in the clinical setting. *Am J Ophthalmol*. 2011;151: 745.e1–751.e1.
11. Stanga PE, Lim JI, Hamilton P. Indocyanine green angiography in chorioretinal diseases: indications and interpretation: an evidence-based update. *Ophthalmology*. 2003;110:15–21, quiz 22–23.
12. Motaghiannezam SM, Koos D, Fraser SE. Differential phase-contrast, swept-source optical coherence tomography at 1060 nm for in vivo human retinal and choroidal vasculature visualization. *J Biomed Opt*. 2012;17:026011.
13. Shin JW, Shin YU, Lee BR. Choroidal thickness and volume mapping by a six radial scan protocol on spectral-domain optical coherence tomography. *Ophthalmology*. 2012;119: 1017–1023.
14. Manjunath V, Taha M, Fujimoto JG, Duker JS. Choroidal thickness in normal eyes measured using Cirrus HD optical coherence tomography. *Am J Ophthalmol*. 2010;150: 325.e1–329.e1.
15. Abrámoff MD, Garvin MK, Sonka M. Retinal imaging and image analysis. *IEEE Rev Biomed Engin*. 2010;3:169–208.
16. Garvin MK, Abramoff MD, Kardon R, Russell SR, Wu X, Sonka M. Intraretinal layer segmentation of macular optical coherence tomography images using optimal 3-D graph search. *IEEE Trans Med Imaging*. 2008;27:1495–1505.
17. Niemeijer M, Staal JS, van Ginneken B, Sonka M, Abramoff AD, eds. Vessel segmentation in 3D spectral OCT scans of the retina. In: *Medical Imaging 2008: Image Processing*. San Diego, CA: SPIE, 2008.
18. Sato Y, Westin CF, Bhalerao A. Tissue classification based on 3D local intensity structures for volume rendering. *IEEE Trans Vis Computer Graphics*. 2000;6:160–179.
19. Sato Y, Nakajima S, Shiraga N, et al. Three-dimensional multi-scale line filter for segmentation and visualization of curvilinear structures in medical images. *Med Image Anal*. 1998;2: 143–168.
20. Frangi AF, Niessen WJ, Vincken KL, et al. Multiscale vessel enhancement filtering. In: Wells WM III, Colchester ACF, Delp SL, et al., eds. *MICCAI Proceedings*. New York, NY: Springer-Verlag; 1998:130–137.
21. Bookstein FL. Principal warps—thin-plate splines and the decomposition of deformations. *IEEE Trans Pattern Anal Mach Intell*. 1989;11:567–585.
22. Dice LR. Measures of the amount of ecologic association between species. *Ecology*. 1945;26:297–302.
23. Schneider U, Kuck H, Inhoffen W, Kreissig I. Indocyanine green angiographically well-defined choroidal neovascularization: angiographic patterns obtained using the scanning laser ophthalmoscope. *Ger J Ophthalmol*. 1995;4:67–74.
24. Yoneya S, Tso MO, Shimizu K. Patterns of the choriocapillaris. A method to study the choroidal vasculature of the enucleated human eye. *Int Ophthalmol*. 1983;6:95–99.
25. Ito YN, Mori K, Young-Duvall J, Yoneya S. Aging changes of the choroidal dye filling pattern in indocyanine green angiography of normal subjects. *Retina*. 2001;21:237–242.
26. Abràmoff MD, Lee K, Niemeijer M, et al. Automated segmentation of the cup and rim from spectral domain OCT of the optic nerve head. *Invest Ophthalmol Vis Sci*. 2009;50: 5778–5784.
27. Agawa T, Miura M, Ikuno Y, et al. Choroidal thickness measurement in healthy Japanese subjects by 3D high-penetration optical coherence tomography. *Graefes Arch Clin Exp Ophthalmol*. 2011;249:1485–1492.
28. Ikuno Y, Kawaguchi K, Nouchi T, Yasuno Y. Choroidal thickness in healthy Japanese subjects. *Invest Ophthalmol Vis Sci*. 2010;51:2173–2176.
29. Esmaeelpour M, Povazay B, Hermann B, et al. 3D 1060-nm OCT: choroidal thickness maps in normal subjects and improved posterior segment visualization in cataract patients. *Invest Ophthalmol Vis Sci*. 2010;51:5260–5266.
30. Spaide RF, Koizumi H, Pozzoni MC. Enhanced depth imaging spectral-domain optical coherence tomography. *Am J Ophthalmol*. 2008;146:496–500.